Contents lists available at SciOpen

Food Science and Human Wellness

journal homepage: https://www.sciopen.com/journal/2097-0765

China Food Publishing Co.

Synthesis of reusable and portable SERS sandpaper based on liquid-liquid interface self-assembly method for stable and ultrasensitive detection of *S*-fenvalerate in foods

Yingfang Zhang[a], Chen Chen[a], Xinyue Wang[a], Xuguang Qiao[a], Ximo Wang[a], Geoffrey I.N. Waterhouse[b,*], Zhixiang Xu[a,*]

[a] *Key Laboratory of Food Processing Technology and Quality Control in Shandong Province, College of Food Science and Engineering, Shandong Agricultural University, Tai'an 271018, China*
[b] *School of Chemical Sciences, The University of Auckland, Auckland 1142, New Zealand*

ARTICLE INFO

Article history:
Received 9 November 2024
Received in revised form 1 December 2024
Accepted 16 December 2024

Keywords:
Surface-enhanced Raman spectroscopy
Liquid-liquid interface self-assembly
Reusable and portable SERS sandpaper
S-Fenvalerate detection

ABSTRACT

Herein, a reusable and portable surface-enhanced Raman spectroscopy (SERS) sandpaper was successfully synthesized for the sensitive detection of *S*-fenvalerate in foods. Commercial sandpapers were decorated with Ag@SiO_2@Au nanoarrays via a liquid-liquid interface self-assembly method. The capacity of sandpaper to float directly on the cyclohexane-water interface allows nanoarrays to be formed directly on it, thereby minimizing stacking issues typically associated with nanoarray assemblies and significantly enhancing the sensitivity of *S*-fenvalerate detection. Moreover, the SERS sandpaper was reusable and portable due to its strong adhesion of the nanoarrays. Under optimized testing conditions, the developed SERS sandpaper method was capable of detecting *S*-fenvalerate, demonstrating a strong linear response within a concentration range of 10^{-7}–10^{3} μmol/L, with a limit of detection of 1.92×10^{-8} μmol/L. The analysis of spiked food samples containing *S*-fenvalerate using the developed SERS sandpaper afforded excellent recoveries (92.2%–109.7%). Additionally, the SERS sandpaper was successfully applied to quantify *S*-fenvalerate in real food samples, with results consistent with analyses conducted using gas chromatography.

1. Introduction

S-Fenvalerate, a highly potent and broad-spectrum type II synthetic pyrethroid insecticide, is widely employed in agriculture to control lepidopterans and sucking pests[1]. Previous reports have found that fruits and vegetables can often contain a high level of *S*-fenvalerate residues. As a result, dietary intake of *S*-fenvalerate residues, particularly from fruits and vegetables, has attracted wide concern[2]. *S*-Fenvalerate poses potential risks to public health, including dizziness, depression, vomiting and abnormal heart rates[3-5]. Accordingly, it is of considerable importance to attain precise and rapid detection of *S*-fenvalerate residues in agricultural products for safeguarding human health.

Presently, various techniques are used for the detection of *S*-fenvalerate detection including high-performance liquid chromatography, gas chromatography and liquid chromatography tandem mass spectrometry[6-10]. Although these methods have high accuracy and selectivity towards *S*-fenvalerate residues, they each have drawbacks including the complicated sample pretreatment procedures and time-consuming analysis routines. In this context, a variety of new methods are now being explored for real-time and rapid detection of *S*-fenvalerate, such as surface-enhanced Raman spectroscopy (SERS), immunoassays, electrochemical sensors and capillary electrophoresis. In particular, SERS has attracted much attention owing to its ultrahigh detection sensitivity and nondestructive analysis[11-16].

* Corresponding authors.
E-mail address: g.waterhouse@auckland.ac.nz (G.I.N. Waterhouse);
zhixiangxu@sina.com (Z.X. Xu)

Peer review under responsibility of Beijing Academy of Food Sciences.

SciOpen Publishing services by Tsinghua University Press

http://doi.org/10.26599/FSHW.2024.9250460

Noble metal nanoparticles (NPs) based on Au and Ag are commonly used in SERS analyses, due to the electromagnetic enhancement mechanism triggered by local surface plasmon resonances (LSPRs) in such noble metal nanomaterials[17]. In general, Ag NPs are considered as the best plasmonic materials for manufacturing SERS substrates[18]. However, due to the oxidation and aggregation of Ag NPs, their application in real-world SERS substrate is currently limited. Uniform coating of Ag NPs with a thin silica shell can markedly increase the stability of Ag NPs without compromising the plasmon resonance activity[19]. However, Au NPs are generally favored in SERS due to their good monodispersity, high chemical stability, ease of synthesis and good SERS performance[20]. However, controlling the separation between NPs to achieve SERS "hot spots" is still a challenge for SERS technology. In recent years, the self-assembly of nanoarrays of plasmonic NPs has attracted attention as a controllable means of generating "hot spots"[21]. One of the frequently employed techniques for producing nanoarrays, liquid-liquid interface self-assembly (LLISA), presents several advantages, including its simplicity and cost-effectiveness[22].

Plasmonic nanoarrays were usually prepared by dipping planar substrates such as silicon wafers and glass microscope slides into liquid-liquid (i.e., oil-water) systems containing noble metal NPs, which often leads to undesirable overlap of 2D nanoarrays[23]. Consequently, finding strategies to prevent the overlap of 2D nanoarrays is of great importance[24]. To better facilitate the widespread applications of 2D nanoarrays and SERS technology, there has been an increasing focus on the design and fabrication of flexible SERS substrates[25]. Sandpaper, possessing micron-scale roughness, low cost, and flexibility, has recently gained popularity in the fabrication of flexible SERS substrates[26-28]. Compared to other flexible materials such as plastic films and filter paper, there are two major advantages of sandpaper: 1) sandpaper can float on aqueous solutions without sinking, which aids the direct formation of nanoarrays on the sandpaper. This can avoid undesirable stacking of nanoarrays during their removal from solution, which is commonly seen for silicon wafers which do not float. Consequently, signal stability of SERS detection is greatly enhanced; 2) sandpaper has inherent roughness, which allows the nanoarrays to firmly adhere to the sandpaper to form a wear-resistant SERS substrate, thereby greatly improving the reusability and storage stability of the SERS substrate, thus enhancing the accuracy of real-time SERS detection[29-30]. Moreover, SERS sandpapers are also lightweight and portable. To date, minimal work has been done relating to the self-assembly of Ag NPs nanoarrays on sandpaper via the LLISA method for the construction of reusable SERS, thus motivating the current investigation.

In this work, a portable and reusable SERS sandpaper based on Ag@SiO_2@Au nanoarrays was constructed for the detection of *S*-fenvalerate in foods. Firstly, Ag@SiO_2@Au NPs were prepared (Scheme 1a). Subsequently, the prepared Ag@SiO_2@Au NPs were directly self-assembled at the cyclohexane/water biphasic interface to form nanoarrays on sandpaper using LLISA (Scheme 1b) for *S*-fenvalerate detection. The obtained SERS sandpaper provided uniform "hot spots" for the detection of *S*-fenvalerate with good signal stability. Consequently, the sensitive detection of *S*-fenvalerate residues in real food samples was realized. This is the first study to apply Ag@SiO_2@Au nanoarrays on sandpaper as a SERS substrate for *S*-fenvalerate detection.

2. Materials and methods

2.1 Synthesis of Ag NPs

Spherical Ag NPs were synthesised using a literature approach[31]. $AgNO_3$ (36 mg) was dissolved in 200 mL of ultrapure water and the resulting solution was heated under vigorous stirring until boiling. Then, 4 mL of a 1 g/100 mL trisodium citrate solution was then rapidly added to the silver nitrate solution under stirring. Subsequently, the mixture was maintained boiling for 1.5 h to ensure total reduction of Ag^+ ions before being cooled with constant agitation.

2.2 Synthesis of Ag@SiO_2 NPs

A total of 0.4 mL of 25% ammonium hydroxide was added to the Ag NPs dispersion, followed by vigorous shaking of the resulting mixture for 20 min. Subsequently, 20 μL of tetraethoxysilane (TEOS) solution in ethanol (at a volume ratio of 1:20) was introduced into the mixture, which was then stirred continuously at room temperature for 8 h. After the mixture was centrifuged at 5 500 r/min for 30 min, the product was washed with anhydrous ethanol twice, then redispersed in ultrapure water (10 mL) for further use.

2.3 Synthesis of Ag@SiO_2@Au NPs

Firstly, the Ag@SiO_2 NPs were aminated using 3-aminopropyltrimethoxysilane (APTMS). Then 5 μL of APTMS was mixed with 10 mL of the dispersion of Ag@SiO_2 NPs and stirred for 10 h. The Ag@SiO_2 NPs with aminated surface were separated through centrifugation at 8 500 r/min for 10 min and subsequently washed twice using anhydrous ethanol. Next, the Au NPs was prepared following the method described by Grabar et al.[32]. Briefly, 0.5 mL of a 1% $HAuCl_4$ solution was mixed with 50 mL of ultrapure water while stirring vigorously for 1 min. Following this, 0.5 mL of a sodium citrate solution (1 g/100 mL) was swiftly added to the mixture. After reaction for 1 min, 0.5 mL of 0.075% $NaBH_4$ in 1% sodium citrate solution was added and the mixture then stirred for 5 min. Subsequently, the Ag@SiO_2@Au NPs were synthesized by mixing 0.5 mL of Au NPs dispersion with 1 mL of aminated Ag@SiO_2 NPs and shaking for 3 h. The product was then centrifuged at 10 000 r/min for 10 min. Ultimately, the mixture was washed twice and re-dispersed in anhydrous ethanol (10 mL).

3. Results and discussion

3.1 Optimization of Ag@SiO_2@Au nanoarray-decorated SERS sandpaper

3.1.1 Optimization of the Ag core size and SiO_2 shell thickness

Different volumes of 1 g/100 mL trisodium citrate solution was optimized to determine the ideal Ag core size. As shown in Figs. 1a and S1, the Raman intensity at 2 226 cm^{-1} attributed to 4-mercaptobenzonitrile (4-MBN) showed an increase with the increasing volume of 1% (*m*/*m*) trisodium citrate solution from 2 to 4 mL and the decrease occurred when the volume of trisodium citrate solution exceeded 4 mL. Consequently, 4 mL of 1 g/100 mL trisodium citrate solution was selected for the preparation of Ag NPs.

Different volumes (2.5, 5, 10, 20, 30 μL) of TEOS ethanol solution (1:20 dilution) were employed to determine the optimal SiO_2 shell thickness. As shown in Figs. 1b and S2, as the volume of the ethanolic TEOS solution (1:20 dilution) increased from 2.5 to 20 μL, there was a gradual increase in Raman intensity at 2 226 cm^{-1} until it reached its peak. The reason of the change in signal was that 4-MBN was in closer proximity to the "hot spots" created between Ag NPs when the SiO_2 shell was relatively thin, resulting in a significant enhancement of the SERS signal for 4-MBN[33]. Upon further increasing the SiO_2 thickness, the excitation laser encountered scattering before it reached the Ag NPs surface, as a result of the extended optical path caused by the presence of the silica shell, which led to a decrease in Raman intensity of the Ag@SiO_2 NPs. Therefore, 20 μL was found to be appropriate for TEOS solution in the synthesis of Ag@SiO_2 NPs.

3.1.2 Optimization of the grit size the sandpaper

The influence of the grit size of sandpaper on the self-assembly process of the Ag@SiO_2@Au nanoarrays was examined. The real images of the Ag@SiO_2@Au nanoarray-decorated SERS sandpapers with different grit sizes were shown in Fig. S3, and the results indicate that only when the roughness of the sandpaper is 2 000 mesh could the nanoarrays achieve complete coverage. Furthermore, Fig. 1c displays the UV-vis absorption spectra of remaining Ag@SiO_2@Au NPs in a water-based solution. The Ag@SiO_2@Au NPs aqueous dispersion exhibited a peak absorbance at 452 nm. Following the addition of 1.5 mL of ethanol, a significant reduction in UV-vis absorbance at 452 nm was observed for each sandpaper with different grit sizes. The efficiency of self-assembly was illustrated in Fig. 1d and calculated using the methodology in prior researches[34-35]. The results showed that 1 000, 1 500 and 2 000 mesh sandpapers achieved self-assembly efficiencies of 64.43%, 70.07%, and 79.58%, respectively. The Raman intensity at 2 226 cm^{-1} reached its maximum when sandpaper with a grit size of 2 000 mesh was used (Figs. 1e, S3 and S4). Therefore, 2 000 mesh was selected as the grit size of the sandpaper for the synthesis of Ag@SiO_2@Au nanoarrays.

3.2 Characterization of the prepared Ag@SiO_2@Au nanoarray-decorated sandpaper

As shown in Fig. 2a, the UV-vis spectra of Ag@SiO_2 NPs exhibited a slight absorption peak centered at 421 nm due to the LSPR of the Ag core. Following the deposition of the Au shell, the UV-vis spectra of the Ag@SiO_2@Au NPs showed two LSPR bands at 421 and 558 nm, which were attributed to the plasmon resonances of the Ag core and Au shell, respectively. Compared to the UV-vis spectrum of the Ag@SiO_2@Au NPs, the absorption band of the Ag@SiO_2@Au nanoarrays exhibited a shift towards longer wavelengths, from 421 to 452 and 558 to 596 nm. The changes in shifts are due to the intense plasmonic interaction between neighboring Ag@SiO_2@Au NPs in the nanoarrays[36], confirming the effective formation of plasmonic nanoarrays on the sandpaper.

The morphology of the Ag@SiO_2@Au nanoarray-decorated sandpaper was examined using SEM. As evidenced in Fig. 2b, the Ag@SiO_2@Au NPs formed densely packed nanoarrays on the surface of the sandpaper with high efficiency. Additionally, the TEM images depicted in Fig. 2c revealed tiny Au NPs firmly attached to the surface of Ag@SiO_2 NPs. Fig. 2d shows the outermost Au NPs in Ag@SiO_2@Au NPs.

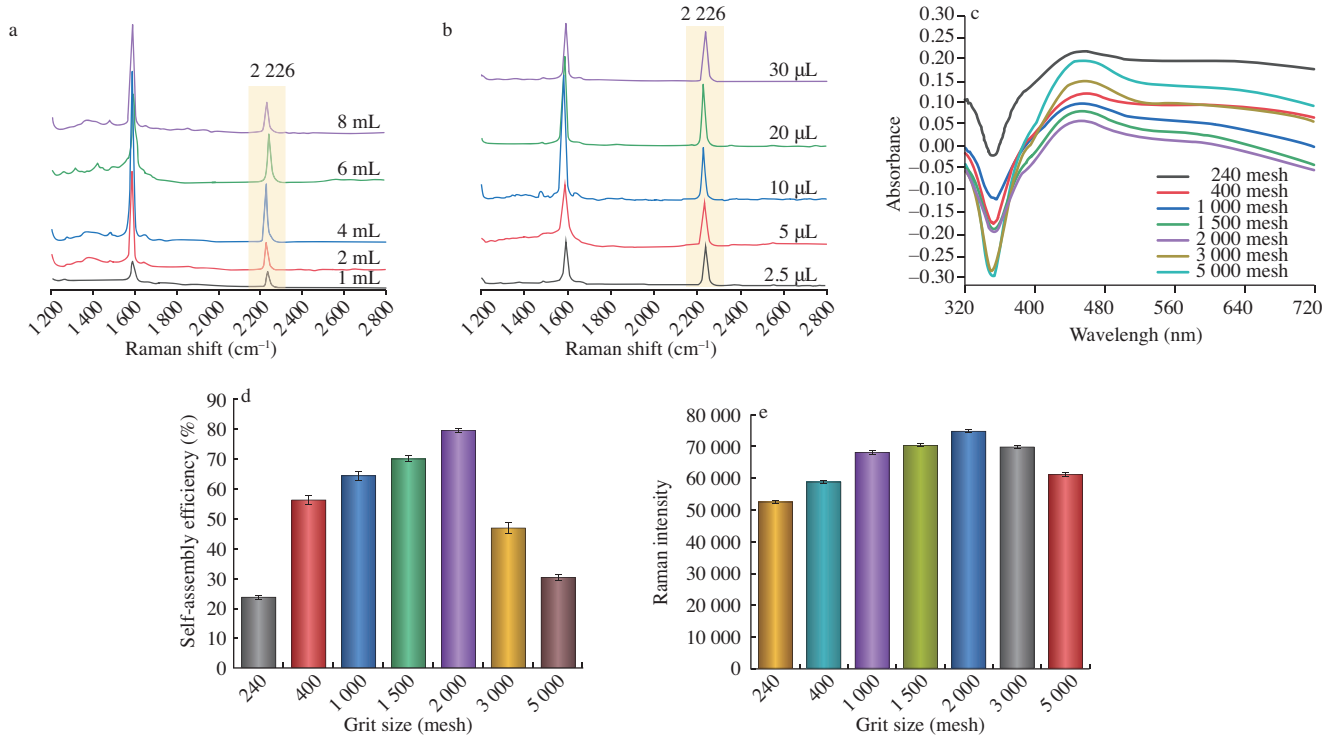

Fig. 1 (a) SERS spectra for Ag NPs prepared with different sizes of Ag core. (b) SERS spectra for Ag@SiO_2@Au NPs prepared with different volumes of TEOS in ethanol (1:20 dilution). (c) UV-Vis absorption spectra for Ag@SiO_2@Au NPs in the aqueous phase after nanoarray formation in the presence of different grit sizes of sandpaper. (d) Self-assembly efficiency of Ag@SiO_2@Au NPs in the presence of different grit sizes of sandpaper. (e) Raman intensity at 2 226 cm^{-1} for Ag@SiO_2@Au nanoarrays prepared using different grit sizes of sandpaper.

The elemental composition of Ag@SiO_2@Au NPs was verified using EDS to map the distribution of elements. The prevailing elements found in Ag@SiO_2@Au were C, N, O, Si, Ag, Si, and Au, which further confirms the successful preparation of Ag@SiO_2@Au NPs (Fig. 2e). Figs. 2f-h shows elemental maps for an individual Ag@SiO_2@Au NP. A concentrated red intensity map for silver was observed within the yellow intensity map for silicon, demonstrating that the Ag NPs were surrounded by silicon dioxide (Figs. 2f and g). The surface of the silicon dioxide was modified with Au NPs, as shown by the green intensity map, suggesting a uniform distribution of Au on the outermost layer of silicon dioxide (Fig. 2h).

3.3 Optimization of the Ag@SiO_2@Au nanoarray-decorated SERS sandpaper method

The study examined the impact of different incubation times (10, 15, 20, 25, 30 min) on the performance of the Ag@SiO_2@Au nanoarray-decorated SERS sandpaper with *S*-fenvalerate. The predominant Raman peaks associated with *S*-fenvalerate molecules were primarily observed within the 600–1 500 cm^{-1} range and the most significant peak observed was at 1 366 cm^{-1}, indicating a C–O stretching vibration[37]. Accordingly, the 1 366 cm^{-1} peak was identified as the characteristic SERS peak associated with *S*-fenvalerate. The maximum Raman intensity at 1 366 cm^{-1} was achieved after a 25-min incubation, followed by stabilization (Figs. 3a and b). As a result, the incubation time of 25 min was chosen for the subsequent experiments.

3.4 Establishment of the Ag@SiO_2@Au nanoarray-decorated SERS sandpaper method for S-fenvalerate detection

SERS spectra were obtained from the Ag@SiO_2@Au nanoarray-decorated sandpaper after exposure to varying concentrations of *S*-fenvalerate solutions, following the optimized testing conditions. The Raman intensity of the distinctive peak of *S*-fenvalerate ($I_{1\,366}$) increased with the logarithm of the *S*-fenvalerate concentration from 10^{-7} to 10^{3} μmol/L (Fig. 3c). The good linear expression was found between $I_{1\,366}$ and the logarithm of *S*-fenvalerate concentration, described by the best-fit equation was $y = 2\,267.30 \lg c + 17\,620.46$ with $R^2 = 0.996\,9$ (Fig. 3d). The limit of detection (LOD) for *S*-fenvalerate was 1.92×10^{-8} μmol/L (based on signal-to-noiseratio was 3)[38]. The results revealed that the prepared SERS sandpaper has high sensitivity for *S*-fenvalerate detection.

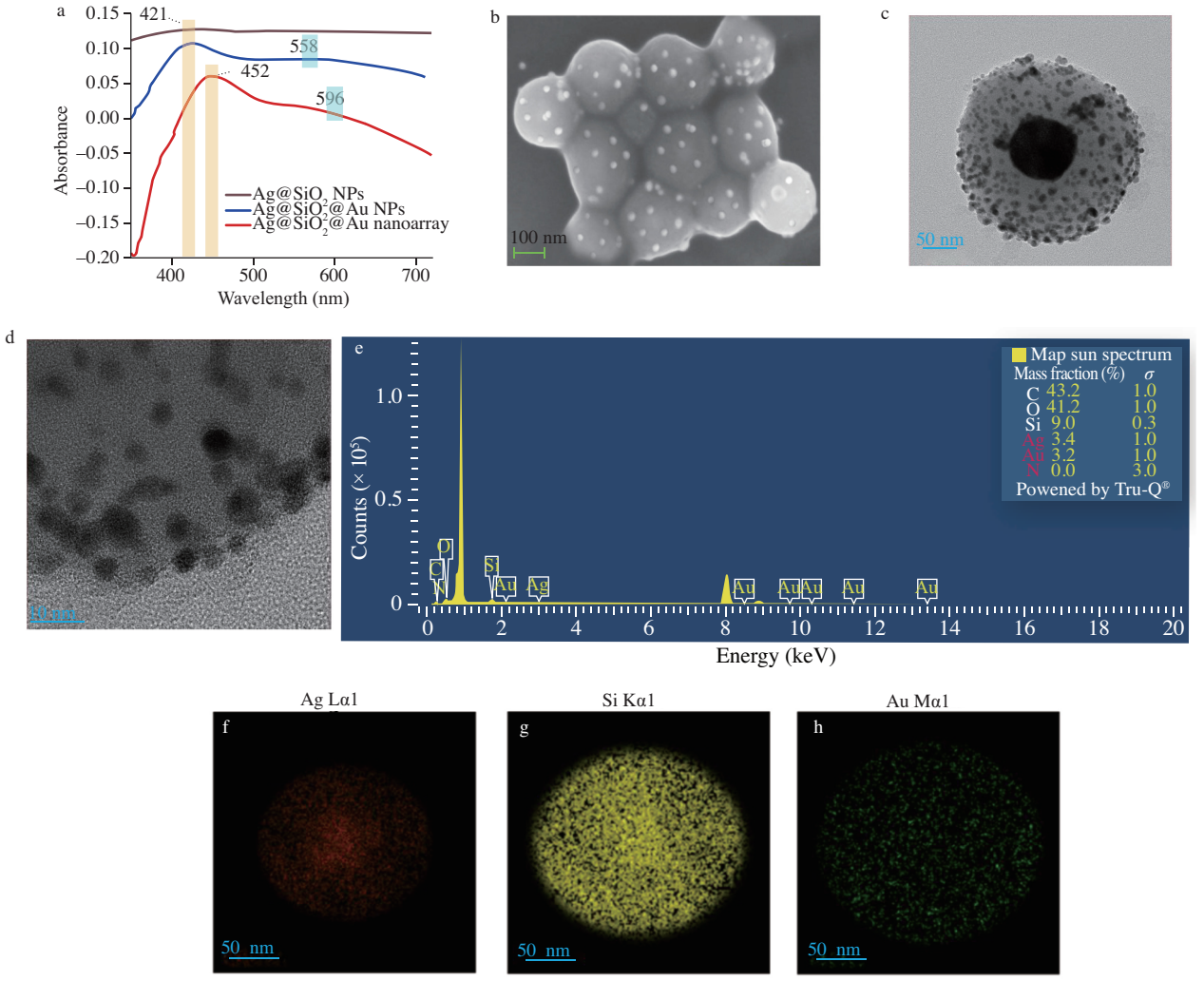

Fig. 2 (a) UV-Vis absorption spectra for Ag@SiO_2 NPs, Ag@SiO_2@Au NPs and Ag@SiO_2@Au nanoarray-decorated sandpaper. (b) Scanning electron microscopy (SEM) image of a Ag@SiO_2@Au nanoarray-decorated sandpaper. (c–d) Transmission electron microscope (TEM) images of Ag@SiO_2@Au nanoarray-decorated sandpaper.(e) Energy dispersive spectroscopy (EDS) spectra of Ag@SiO_2@Au nanoarray-decorated sandpaper. (f–h) Elemental mapping images of Ag@SiO_2@Au nanoarray-decorated sandpaper.

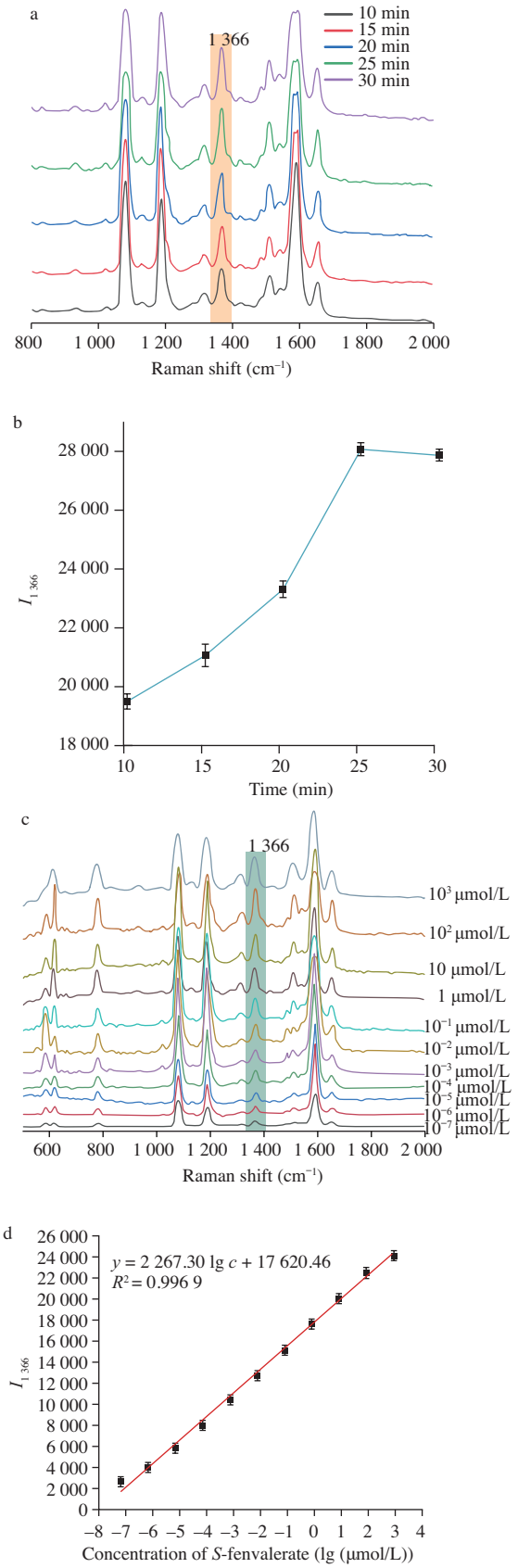

Fig. 3 (a) Raman intensity at 1 366 cm^{-1} with different incubation times. (b) Plot of Raman intensity at 1 366 cm^{-1} versus incubation time. (c) SERS spectra for *S*-fenvalerate at different concentrations. (d) Linear relationship between $I_{1\,366}$ and the logarithm of the *S*-fenvalerate concentration over the range 10^{-7}–10^{3} μmol/L.

3.5 SERS enhancement effect of Ag@SiO_2@Au nanoarray-decorated SERS sandpaper

To investigate the enhancement effect of SERS, Raman spectra for Ag NPs, Ag@SiO_2 NPs, Ag@SiO_2@Au NPs, Ag@SiO_2@Au nanoarray-decorated sandpaper of 4-MBN (0.1 mol/L in ethanol solvent) at 2 226 cm^{-1} were gathered. The Raman signals for Ag NPs and Ag@SiO_2 NPs were weak (Fig. S5). In contrast, the Raman intensity of Ag@SiO_2@Au NPs and Ag@SiO_2@Au nanoarrays was strong. Furthermore, the Raman intensity at 2 226 cm^{-1} of Ag@SiO_2@Au nanoarrays was approximately twice that of Ag@SiO_2@Au NPs, demonstrating that the "hot spots" created in the nanoarrays on sandpaper improved the SERS enhancement effect.

3.6 Uniformity,reproducibility,storage stability and anti-interference of Ag@SiO_2@Au nanoarray-decorated SERS sandpaper

To evaluate the signal uniformity of the developed SERS sandpaper, 20 randomly spots were selected within an area of 40 μm × 40 μm on the Ag@SiO_2@Au nanoarray-decorated SERS sandpaper. The results showed that the Raman intensity at 1 366 cm^{-1} did not show any significant difference as the location was changed, with the trend in the signal due to 4-MBN at 2 226 cm^{-1} also being similar, demonstrating the point-to-point signal stability of the developed SERS sandpaper was good (Fig. 4a).

The spectra were gathered from 40 spots chosen at random across 5 sets of Ag@SiO_2@Au nanoarray-decorated SERS sandpaper to assess the reproducibility of the fabricated SERS sandpaper. As can be seen from Fig. 4b, the SERS intensities at 1 366 cm^{-1} had a low RSD of 4.52%. It can be inferred that the proposed SERS sandpaper offered good batch-to-batch reproducibility.

The Raman intensity at 2 226 cm^{-1} of the Ag@SiO_2@Au nanoarray-decorated sandpaper and Ag@SiO_2@Au nanoarray-decorated silicon wafer at various storage times were compared to evaluate the storage stability of the prepared SERS sandpaper. The Raman intensity at 2 226 cm^{-1} of the Ag@SiO_2@Au nanoarray-decorated sandpaper for 4-MBN decreased only by 11.5% (over 30 days), whilst the Raman intensity for Ag@SiO_2@Au nanoarray-decorated silicon wafer decreased 33.9%, implying the developed sandpaper possessed superior storage stability (Fig. 4c).

Furthermore, in order to investigate the anti-interference properties of the SERS sandpaper, a range of possible interfering agents were added into 10^3 μmol/L *S*-fenvalerate solutions, including any interferent (Fig. 4d) at concentrations 100 times higher than normal. The results showed negligible change in the presence of the interferent. Therefore, the anti-interference ability of the constructed SERS sandpaper was excellent.

3.7 Reusability, accuracy and applicability of the Ag@SiO_2@Au nanoarray-decorated SERS sandpaper

Preparing reusable SERS sandpaper is necessary to lower detection costs, thus we investigated its reusability. The cleaning technique for the SERS sandpaper was simple, as indicated in Scheme 1c. Briefly, the used sandpaper was placed in a tiny petri dish with anhydrous ethanol and soaked it for 5 min, then shaken and finally dried it at room

temperature for reuse. Fig. 4e indicates that there was a minimal amount of *S*-fenvalerate remaining following the recycling process, with the initial Raman intensity at 1 366 cm^{-1} retained after 5 repeat use cycles[39]. The result shows that the Ag@SiO_2@Au nanoarray-decorated SERS sandpaper had good reusability. Therefore, the Ag@SiO_2@Au nanoarray-decorated sandpaper can be used as a reusable SERS substrate for detection of *S*-fenvalerate, offering advantages compared to other types of flexible SERS substrates.

Next, recovery experiments were conducted using spiked spinach and pear samples to further validate the accuracy of the prepared SERS sandpaper for *S*-fenvalerate detection. As shown in Table 1, the recovery values of *S*-fenvalerate in the spiked pear and spinach samples were in the range of 95.01%−102.44% with RSD of 1.88%–3.02%, confirming good reliability and practicality of the developed SERS sandpaper. That might be related to the outstanding performance of sandpaper. Since sandpaper has the ability to float at cyclohexane-water interfaces, the procedure for decorating the sandpaper with Ag@SiO_2@Au nanoarrays was very simple compared with previous works[40], thus greatly improving the accuracy of the SERS detection method.

To evaluate the practical utility of the SERS sandpaper for real samples, the SERS sandpaper method and GC detection method were utilized to measure the concentration of *S*-fenvalerate in celery cabbage, asparagus lettuce, and peach. The concentration of *S*-fenvalerate in the

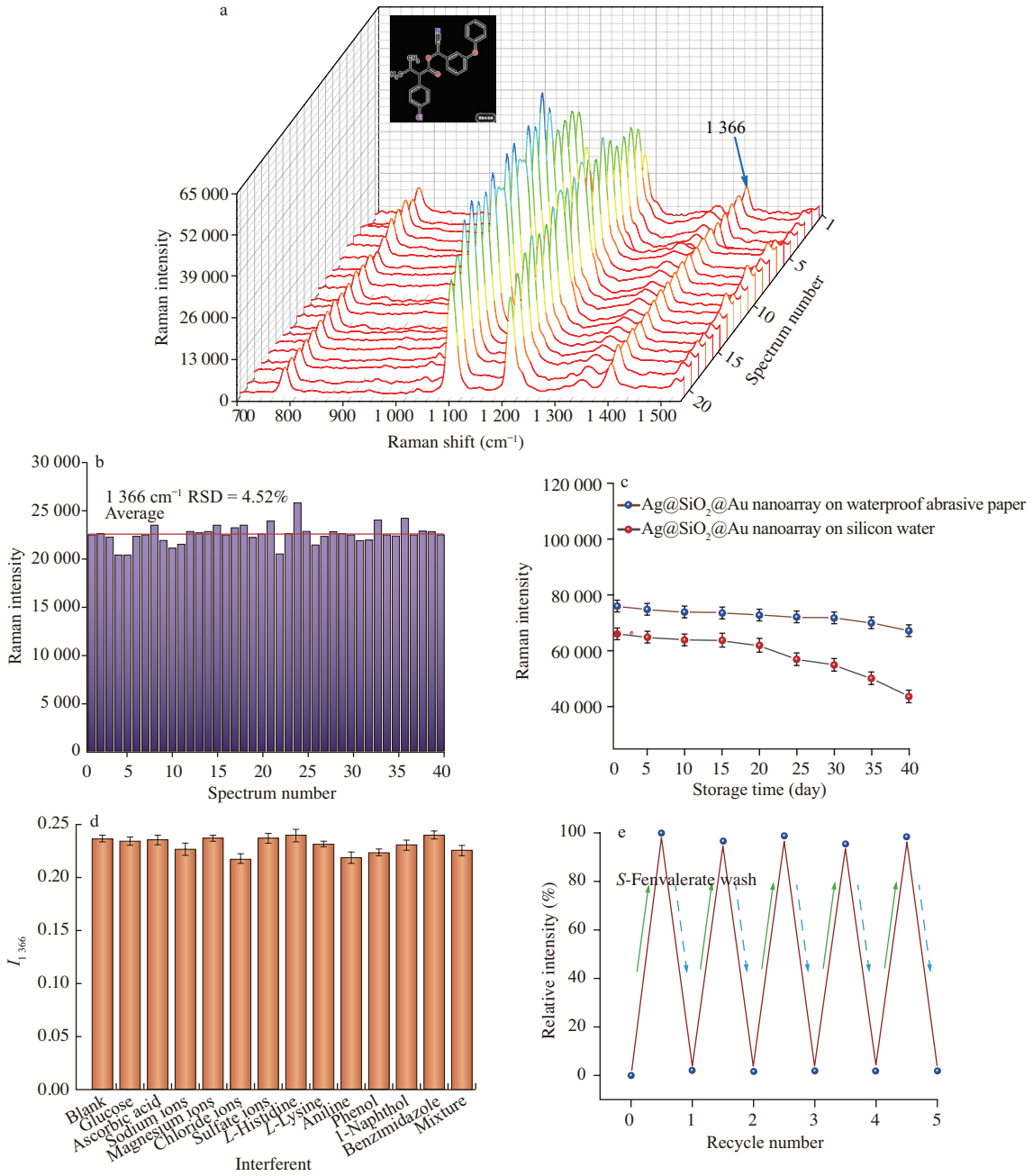

Fig. 4 (a) Raman intensity at 1 366 cm^{-1} from 20 randomly selected spots in two areas (each 20 μm × 20 μm) of the Ag@SiO_2@Au nanoarray-decorated sandpaper. The inset shows the structure of *S*-fenvalerate. (b) Raman intensity at 1 366 cm^{-1} from 40 randomly selected spots in 5 batches of Ag@SiO_2@Au nanoarray-decorated sandpaper. (c) Raman intensity at 2 226 cm^{-1} for Ag@SiO_2@Au nanoarray-decorated sandpaper after different storage times. (d) Raman intensity at 1 366 cm^{-1} for the Ag@SiO_2@Au nanoarray-decorated sandpaper in the presence of different possible interferents. (e) Relative SERS intensities of *S*-fenvalerate (10^3 μmol/L) with recycling of the SERS sandpaper.

three samples determined using the Ag@SiO_2@Au nanoarrays decorated SERS sandpaper were 2.29×10^{-2}, 1.88×10^{-2}, 5.41×10^{-2} μg/g, respectively. The contents obtained using the GC method were 2.31×10^{-2}, 1.76×10^{-2}, 5.26×10^{-2} μg/g, respectively (Table 2). The analysis results showed that no significant differences were found between two methods, demonstrating the prepared SERS sandpaper is suitable for the rapid monitoring of *S*-fenvalerate in real samples.

Table 1
Recovery tests of *S*-fenvalerate in spiked food samples using the SERS sandpaper.

Sample	Original level (μg/g)	Added level (10^{-1} μg/g)	Found level (10^{-1} μg/g)	Recovery (± RSD, %)
Pear	0	1	0.95	95.01 ± 3.02
		50	50.56	101.12 ± 2.05
		100	98.96	98.95 ± 1.88
Spinach	0	1	0.98	97.99 ± 2.83
		50	51.22	102.44 ± 2.67
		100	100.77	100.76 ± 1.93

Table 2
Performance comparison of the SERS sandpaper method and a GC method for the detection of *S*-fenvalerate in real food samples.

Sample	Found level by SERS sandpaper (10^{-2} μg/g)	Found level by GC (10^{-2} μg/g)
Celery cabbage	2.29[a]	2.31[a]
Asparagus lettuce	1.88[a]	1.76[a]
Peach	5.41[a]	5.26[a]

Note: Different lowercase letters in the same column indicate significant differences ($P < 0.05$).

3.8 Analytical performance of Ag@SiO_2@Au nanoarray-decorated SERS sandpaper

The comparison of the performance of the Ag@SiO_2@Au nanoarray-decorated SERS sandpaper with other previous methods for *S*-fenvalerate detection was shown in Table S1. The linear detection range of the developed SERS sandpaper was much wider and the LOD was much lower, suggesting that the Ag@SiO_2@Au nanoarray-decorated SERS sandpaper method can be applied for the sensitive detection of *S*-fenvalerate. Moreover, the constructed SERS sandpaper was extremely portable, with the "hot spots" generated on it not easily destroyed due to the strong attachment of the nanoarrays to the sandpaper.

4. Conclusions

A reusable and portable SERS sandpaper based on Ag@SiO_2@Au nanoarrays was constructed for precise quantification of *S*-fenvalerate in foods. The established SERS sandpaper possessed excellent uniformity, sensitivity, reusability and storage stability and offered a wide linear range with low LOD for *S*-fenvalerate detection. Furthermore, the fabricated SERS sandpaper could be readily applied for the *S*-fenvalerate detection in actual samples (e.g., celery cabbage, asparagus lettuce, and peach). This work provided a new insight for developing more stable and wearable sensors for on-site detection in the future.

Conflict of interest statement

Geoffrey I.N. Waterhouse is a scientific editor for *Food Science and Human Wellness* and was not involved in the editorial review or the decision to publish this article. The authors declare that they have no known competing financial interests or personal relationships that could have appeared to influence the work reported in this paper.

Acknowledgements

This work was financially supported by the Key R&D Program of Shandong Province, China (2023CXGC010712).

Appendix A. Supplementary data

Supplementary data associated with this article can be found, in the online version, at http://doi.org/10.26599/FSHW.2024.9250460.

References

[1] J. Liu, Q. Zhang, W. Zhang, et al., Development of a uorescence-linked immunoassay based on quantum dots for fenvalerate, Food Agr. Immunol. 25 (2014) 82-93. https://doi.org/10.1080/09540105.2012.749220.

[2] T.S. Ranjani, G.K. Pitchika, K. Yedukondalu, et al., Phenotypic and transcriptomic changes in zebrafish (*Danio rerio*) embryos/larvae following cypermethrin exposure, Chemosphere 249 (2020) 126148. https://doi.org/10.1016/j.chemosphere.2020.126148.

[3] C. Giulioni, V. Maurizi, D. Castellani, et al., The environmental and occupational influence of pesticides on male fertility: a systematic review of human studies, Andrology 10 (2022) 1250-1271. https://doi.org/10.1111/andr.13228.

[4] L. Dalsagera, F.L. Bettina, N. Bilenbergb, et al., Maternal urinary concentrations of pyrethroid and chlorpyrifos metabolites and attention deficit hyperactivity disorder (ADHD) symptoms in 2-4-year-old children from the Odense Child Cohort, Environ. Res. 176 (2019) 108533. https://doi.org/10.1016/j.envres.2019.108533.

[5] M.A. Martínez, J.L. Rodríguez, L.T. Bernardo, et al., Oxidative stress and related gene expression effects of cyfluthrin in human neuroblastoma SH-SY5Y cells: protective effect of melatonin, Environ. Res. 177 (2019) 108579. https://doi.org/10.1016/j.envres.2019.108579.

[6] M.M. Galera, M.D.G. Garc, R.S. Valverde, Determination of nine pyrethroid insecticides by high-performance liquid chromatography with post-column photoderivatization and detection based on acetonitrile chemiluminescence, J. Chromatogr. A 1113 (2006) 191-197. https://doi.org/10.1016/j.chroma.2006.02.013.

[7] M.R. Cao, J. Wang, M.T. Wang, et al., Simultaneous detection of 22 mycotoxins in grape by QuEChERS and ultra-high performance liquid chromatography coupled with quadrupole/orbitrap high-resolution mass spectrometry, J. Future Foods 44 (2024) 369-375. https://doi.org/10.1016/j.jfutfo.2023.11.009.

[8] Q. Chang, T. Feng, S. Song, et al., Analysis of eight pyrethroids in water samples by liquid-liquid microextraction based on solidification of floating organic droplet combined with gas chromatography, Microchim. Acta 171 (2010) 241-247. https://doi.org/10.1007/s00604-010-0430-1.

[9] T. Tagami, K. Kajimura, K. Yamasaki, et al., Simple and rapid determination of cypermethrin and fenvalerate residues in kampo products by gas chromatography-mass spectrometry with negative chemical ionization, J. Health Sci. 55 (2009) 777-782. https://doi.org/10.1248/jhs.55.777.

[10] D.B. Martinez, P.P. Vazquez, M.M. Galera, et al., Determination of pyrethroid insecticides in vegetables with liquid chromatography using detection by electrospray mass spectrometry, Chromatographia 63 (2006) 487-491. https://doi.org/10.1365/s10337-006-0777-y.

[11] C. Chen, X.Y. Wang, X.M. Wang, et al., "One-Pot" readout cyano-programmable sers-encoded platform enables ultrasensitive and interference-free detection of multitarget bioamines, Anal. Chem. 96 (2024) 12862-12874. https://doi.org/10.1021/acs.analchem.4c02582.s001.

[12] C. Chen, Y.F. Zhang, X.M. Wang, et al., A core-satellite self-assembled SERS aptasensor containing a "biological-silent region" Raman tag for the accurate and ultrasensitive detection of histamine, Food Sci. Hum. Wellness 13 (2024) 1029-1039. https://doi.org/10.26599/fshw.2022.9250089.

[13] L. Jiang, M.M. Hassan, S. Ali, et al., Volving trends in SERS-based techniques for food quality and safety: a review, Trends Food Sci. Tech. 112 (2021) 225-240. https://doi.org/10.1016/j.tifs.2021.04.006.

[14] W.C. Seo, W.C. Wei, Surface-enhanced Raman spectroscopy for emerging contaminant analysis in drinking water, Front. Env. Sci. Eng. 57 (2022) 17. https://doi.org/10.1007/s11783-023-1657-5.

[15] Q.Q. Li, H.Q. Huo, Y. Wu, et al., Design and synthesis of SERS materials for *in vivo* molecular imaging and biosensing, Adv. Sci. 10 (2023) e2202051. https://doi.org/10.1002/advs.202202051.

[16] Y.J. Sun, D.Y. Lou, W. Liu, et al., SERS labels for optical anticounterfeiting: structure, fabrication, and performance, Adv. Opt. Mater. 6 (2023) 2201594. https://doi.org/10.1002/adom.202201549.

[17] T.H. Xie, Z.J. Cao, Y.J. Li, et al., Highly sensitive SERS substrates with multi-hot spots for on-site detection of pesticide residues, Food Chem. 381 (2022) 132208. https://doi.org/10.1016/j.foodchem.2022.132208.

[18] L.M. Yin, T.Y. You, M. Arslan, et al., Dual-layers Raman reporter-tagged Au@Ag combined with core-satellite assemblies for SERS detection of Zearalenone, Food Chem. 429 (2023) 136834. https://doi.org/10.1016/j.foodchem.2023.136834.

[19] M. Wan, H. Zhao, Z. Wang, et al., Fabrication of Ag modified SiO_2 electrospun nanofibrous membranes as ultrasensitive and high stable SERS substrates for multiple analytes detection, Colloid Interfac. Sci. 416 (2021) 1047-1056. https://doi.org/10.1016/j.colcom.2021.100428.

[20] M. Wan, H. Zhao, L. Peng, et al., Loading of Au/Ag bimetallic nanoparticles within and outside of the flexible SiO_2 electrospun nanofibers as highly sensitive, stable, repeatable substrates for versatile and trace SERS detection, Polymers 12 (2020) 3008. https://doi.org/10.3390/polym12123008.

[21] S.B. Jamali, M.A. Khaskheli, M.I. Abro, et al., Confirming the SERS enhancement at large mapping area using self-assembly of silver nanocube at liquid-liquid cyclohexane/water interface, J. Mol. Liq. 326 (2021) 115365. https://doi.org/10.1016/j.molliq.2021.115365.

[22] S.L. Xu, H.F. Li, M. Guo, et al., Liquid-liquid interfacial self-assembled triangular Ag nanoplate-based high-density and ordered SERS-active arrays for the sensitive detection of dibutyl phthalate (DBP) in edible oils, The Analyst 146 (2021) 4858. https://doi.org/10.1039/d1an00713k.

[23] T.T. Pan, D.W. Sun, H.B. Pu, et al., Simple approach for the rapid detection of alternariol in pear fruit by surface-enhanced Raman scattering with pyridine-modified silver nanoparticles, J. Agri. Food Chem. 66 (2018) 2180-2187. https://doi.org/10.1021/acs.jafc.7b05664.

[24] S.Z. Oo, R.Y. Chen, S. Siitonen, et al., Disposable plasmonic plastic SERS sensor, Opt. Express 21 (2013) 1848491. https://doi.org/10.1364/oe.21.018484.

[25] J. Li, K.R. Chen, Y. Su, et al., Paper-based biosensors based on multiple recognition modes for visual detection of microbially contaminated food, J. Future Foods 41 (2024) 61-70. https://doi.org/10.1016/j.jfutfo.2023.05.007.

[26] Z.Y. Yang, H.M. Liu, Y.R. Tian, et al., Synergistic effect of a "stellate" mesoporous SiO_2@Au nanoprobe and coffee-ring-free hydrophilic-hydrophobic substrate assembly in an ultrasensitive SERS-based immunoassay for a tumor marker, J. Mater. Chem. 8 (2020) 2142-2154. https://doi.org/10.1039/c9tc05646g.

[27] D.D. Yuan, S. Chen, Y.N. Wu, et al., A facile surface enhanced Raman scattering substrate based on silver deposited sandpaper, Mod. Phys. Lett. B 33 (2019) 1950239. https://doi.org/10.1142/s0217984919502397.

[28] Y.Y. Du, H.M. Liu, Y.R. Tian, et al., Recyclable SERS-based immunoassay guided by photocatalytic performance of Fe_3O_4@TiO_2@Au nanocomposites, Biosensors 10 (2020) 25. https://doi.org/10.3390/bios10030025.

[29] A. Mohan, L. Chandran, K.G. Gopchandran, Fabrication of flexible AgNW@R-PDMS SERS substrates by sandpaper-assisted lithography for surface swab capture of fungicides, ACS Appl. Opt. Mater. 2 (2024) 268633937. https://doi.org/10.1021/acsaom.4c00006.s001.

[30] Y.H. Tan, Z.Y. Zhou, Y.T. Xu, et al., Detection of organic dyes using Ag NPAs/SMP SERS substrate produced via sandpaper template-assisted lithography and liquid-liquid interface self-assembly, Anal. Bioanal. Chem. 416 (2024) 1047-1056. https://doi.org/10.1007/s00216-023-05094-8.

[31] D.D. Deng, H. Yang, C. Liu, et al., Ultrasensitive detection of diclofenac in water samples by a novel surfaceenhanced Raman scattering (SERS)-based immunochromatographic assay using Ag^{MBA}@SiO_2-Ab as immunoprobe, Sensor. Actuat. B: Chem. 283 (2019) 563-570. https://doi.org/10.1016/j.snb.2018.12.076.

[32] K.C. Grabar, K.J. Allison, B.E. Baker, et al., Two-dimensional arrays of colloidal gold particles: a flexible approach to macroscopic metal surfaces, Langmuir 12 (1996) 2353-2361. https://doi.org/10.1021/la950561h.

[33] X. Chen, L. Zhu, Z. Ma, et al., Ag nanoparticles decorated ZnO nanorods as multifunctional SERS substrates for ultrasensitive detection and catalytic degradation of Rhodamine B, Nanomaterials 12 (2022) 2394. https://doi.org/10.3390/nano12142394.

[34] J.B. Edel, A.A. Kornyshev, A.R. Kucernak, et al., Fundamentals and applications of self-assembled plasmonic nanoparticles at interfaces, Chem. Soc. Rev. 45 (2016) 1581-1596. https://doi.org/10.1039/c5cs00576k.

[35] Y. Xu, M.P. Konrad, W.W. Lee, et al., A method for promoting assembly of metallic and nonmetallic nanoparticles into interfacial monolayer films, Nano Lett. 16 (2016) 5255-5260. https://doi.org/10.1021/acs.nanolett.6b02418.

[36] L.B. Zhong, J. Yin, Y.M. Zheng, et al., Self-assembly of Au nanoparticles on PMMA template as flexible, transparent, and highly active SERS substrates, Anal. Chem. 86 (2014) 6262-6267. https://doi.org/10.1021/ac404224f.

[37] H.J. Li, Y. Wang, L. Yue, et al., Fabrication of pollutant-resistance SERS imprinted sensors based on SiO@TiO_2@Ag composites for selective detection of pyrethroids in water, J. Phys. Chem. Solids 138 (2020) 109254. https://doi.org/10.1016/j.jpcs.2019.109254.

[38] C. Chen, X.M. Wang, Y.F. Zhang, et al., A molecularly-imprinted SERS sensor based on a TiO_2@Ag substrate for the selective capture and sensitive detection of tryptamine in foods, Food Chem. 394 (2022) 133536. https://doi.org/10.1016/j.foodchem.2022.133536.

[39] S.H. Mao, F.B. Pei, S.S. Feng, et al., Detection of trace Rhodamine B using stable, uniformity, and reusable SERS substrate based on Ag@SiO_2-Au nanoparticles, Colloid. Surfaces A 657 (2023) 130595. https://doi.org/10.1016/j.colsurfa.2022.130595.

[40] Y.F. Zhang, C. Chen, R.Q. Wang, et al., Internal standard-based self-assembly Ag@4-MBN@Ag nanoarray SERS ratio sensor for sensitive detection of deltamethrin in foods, Sensors Actuat. B: Chem. 412 (2024) 135786. https://doi.org/10.1016/j.snb.2024.135786.